Supporting Information

Electrochemical conversion of CO_2 to syngas with a stable H_2/CO ratio in a wide potential range over ligand-engineered metal–organic frameworks

Lin Cao[a], Xuefeng Wu[a], Yuanwei Liu[a], Fangxin Mao[a], Yingli Shi[a], Jiayu Li[b], Minghui Zhu[b], Sheng Dai[c], Aiping Chen[a], Peng Fei Liu[a*], Hua Gui Yang[a*]

[a] Key Laboratory for Ultrafine Materials of Ministry of Education, Shanghai Engineering Research Center of Hierarchical Nanomaterials, School of Materials Science and Engineering, East China University of Science and Technology, 130 Meilong Road, Shanghai 200237, China.

[b] Key Laboratory of Chemical Engineering, School of Chemical Engineering, East China University of Science and Technology, 130 Meilong Road, Shanghai 200237, China.

[c] Key Laboratory for Advanced Materials and Feringa Nobel Prize Scientist Joint Research Center, Institute of Fine Chemicals, School of Chemistry and Molecular Engineering, East China University of Science and Technology, 130 Meilong Road, Shanghai 200237, China.

Emails: hgyang@ecust.edu.cn; pfliu@ecust.edu.cn

Experimental Section

Chemicals. Zinc nitrate hexahydrate ($Zn(NO_3)_2 \cdot 6H_2O$, 99.5%) and Zinc powder were purchased from Sinopharm Chemical Reagent Co., Ltd. N-dimethylformamide (DMF, 99.8%) was purchased from J&K Scientific Co., Ltd. 1,3,5-benzenetricarboxylic acid (H_3BTC, 95%) and 1,4-benzenedicarboxylate (H_2BDC, 98%) were obtained from Sigma-Aldrich. Potassium bicarbonate ($KHCO_3$) and isopropyl alcohol (AR, ≥99.0%) were obtained from Shanghai Chemical Reagent Co., Ltd. Potassium hydroxide (KOH, 85%) were purchased from Yong Hua Chemical Co., Ltd. Nafion (5 wt% in a mixture of lower aliphatic alcohols and water) was obtained from Sigma-Aldrich. Carbon dioxide (CO_2, 99.9999%) and Argon gas (Ar, 99.9999%) were bought from Shanghai Jiajie Special Gas Co., Ltd. Gas diffusion electrodes (GDE, Sigracet 28 BC) was from the Fuel Cell Store. All chemicals were used as received without further purification and all water used for synthesis and analysis was purified to >18.2 MΩ cm by the Millipore system.

Preparation of Zn-BTC. Typically, 5 mmol of H_3BTC and 5 mmol of $Zn(NO_3)_2 \cdot 6H_2O$ were dissolved using 50 mL of DMF. Then, the solution was heated in a microwave oven on medium heat for one hour. After that, the mixture was left at room temperature for 30 min to cool down. Finally, the precipitate was washed with DMF several times and dried in a vacuum at 60 °C.

Preparation of Zn-BDC. Similar to Zn-BTC, 5 mmol of H_2BDC and 5 mmol of $Zn(NO_3)_2 \cdot 6H_2O$ were dissolved using 50 mL of DMF. Then, the solution was heated in

a microwave oven on medium heat for one hour. After that, the mixture was left at room temperature for 30 min to cool down. Finally, the precipitate was washed with DMF several times and dried in a vacuum at 60 °C.

Characterizations. The morphologies of all samples were analyzed by scanning electron microscopy (SEM, Hitachi S4800). The corresponding crystal structure was characterized by X-ray diffraction (XRD, D/max2550V). Scanning transmission electron microscopy (STEM) and transmission electron microscopy (TEM) characterizations were performed using ThermoFisher Talos F200X. High angle annular dark field (HAADF-STEM) images were recorded using a convergence semi-angle of 11 mrad, and inner and outer collection angles of 59 and 200 mrad, respectively. Energy-dispersive X-ray spectroscopy (EDS) was carried out using 4 in-column Super-X detectors. The chemical states of the elements were examined by X-ray photoelectron spectroscopy (XPS, Kratos Axis Ultra DLD), and the energy corrections were calibrated by referencing the C 1s peak of adventitious carbon to 284.8 eV. Volumetric CO_2 adsorption measurement (Micromeritics ASAP 2020) was analyzed at 298 K and 1 atm. FTIR spectroscopy was characterized on a Nicolet 6700 spectrometer with a spectral range of 4000-400 cm^{-1}. XAFS spectra at the Zn K-edge were performed on the 1W1B beamline station of the Beijing Synchrotron Radiation Facility (BSRF), China. The electron beam energy was about 2.5 GeV and the stored current was about 200 mA. A 38-pole wiggler with the maximum magnetic field of 1.2 T inserted in the straight section of the storage ring was used. XAFS data were collected using a double-crystal Si (111) monochromator. The raw data analysis was performed

using the IFEFFIT software package according to the standard data analysis procedures.

In situ attenuated total reflection surface-enhanced infrared absorption spectroscopy (ATR-SEIRAS) was measured at PerkinElmer spectrum 100 spectrometers equipped with a mercury cadmium telluride (MCT) detector, a variable angle specular reflectance accessory (VeemaxIII, Pike Technologies) and a one-compartment cell (LingLu Instruments Co., China) including a Pt counter electrode (CE), an Ag/AgCl reference electrode (RE), a gas inlet port and a gas outlet port. A catalyst-coated Si ATR crystal with Au film underlayer is placed in the cell as the working electrode. The Au film underlayer is prepared following a variation of reported electroless Au deposition techniques[1]. A CHI1242C potentiostat was employed to record the electrochemical response. During the experiments, the CO_2 gas was kept flowing into the solution at a flow rate of 20 standard cubic centimeters per minute (sccm). An open-circuit voltage (OCV) spectra were collected first. The spectra were collected step-wisely from −1.2 to −1.8 V vs. RHE with a dwell time of 5 minutes at each potential.

Preparation of working electrode. The catalyst ink was prepared by ultrasonically dispersing of 3 mg sample and 80 μL Nafion solution (5 wt%) in 1 mL isopropanol for 30 min. The ink was sprayed on a GDE (Sigracet 28 BC) using an air-brush. The samples electrodes were dried for at least 24 h at room temperature in a vacuum chamber before operation.

Electrochemical reduction of CO_2. All CO_2 electrolysis experiments were performed using a three-electrode set-up in a flow-cell configuration connected to an

electrochemical workstation (CHI 660). An Ag/AgCl (3.5 M KCl) and a piece of Ni foam were used as a reference and counter electrodes, respectively. Electrode potentials in the study were converted to the reversible hydrogen electrode (RHE) according to the following equation without *iR* correction, $E_{(vs.\ RHE)} = E_{Ag/AgCl} + 0.059 \times pH + 0.205$ (with *iR* correction: $E_{(vs.\ RHE)} = E_{Ag/AgCl} + 0.059 \times pH + 0.205 - 0.8 \times iR$). The linear sweep voltammetry (LSV) with a scan rate of 10 mV s^{-1} was performed in 1 M $KHCO_3$ aqueous solution with the CO_2/Ar flow at a rate of 40 sccm. The current density was calculated by normalizing the current to the corresponding geometric surface area (0.5 cm^2).

Products analysis. The gas products were analyzed by gas chromatography (GC), equipped with the flame ionization detector (FID for CO and hydrocarbons) and a thermal conductivity detector (TCD for H_2). The CO_2 gas was continuously purged at an average rate of 40 sccm into the cathodic compartment and was routed into the gas chromatograph (RAMIN, GC2060). Argon is the carrier gas. Liquid products were detected by quantitative ^1H nuclear magnetic resonance (NMR) technique (Varian 700MHz spectrometer (16.4 T).

Assuming that two electrons are needed to produce one methane molecule, the FE, the partial current densities of CO formation and the turnover frequencies of CO were calculated as below:

$$FE = \frac{2FvGP_0}{i_{total}RT} \times 100\%$$

,

where v=volume concentration of CO obtained from gas chromatography (GC) data, p_0 = 1.013 bar and T = 298.15 K, G = 40 mL min^{-1} is the CO_2 flow rate, i_{total} (mA) =

steady-state cell current, F = 96485 C mol^{-1}, R = 8.314 J mol^{-1} K^{-1}.

then:

$$j_{CO} = FE_{CO} \times i_{total} \times (electrode\ area)^{-1}.$$

Then:

$$TOF\ (s^{-1}) = \frac{I_{CO}/nF}{m_{cat} \times \omega / M_{Zn}}$$

Where I_{CO} = partial current for CO production, A; n = the number of electrons transferred for CO production, which is 2 for CO; F = Faradaic constant, 96485 C mol^{-1}; m_{cat}: the mass of catalyst on the electrode, g; ω = Zn loading in the catalyst; $M_{Zn} = 65.41\ g\ mol^{-1}$, the atomic mass of Zn.[2]

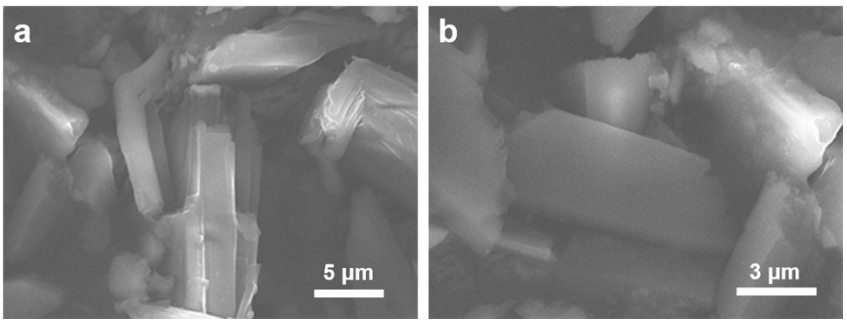

Fig. S1. SEM images of Zn-BDC at different magnifications showing a rod-like morphology.

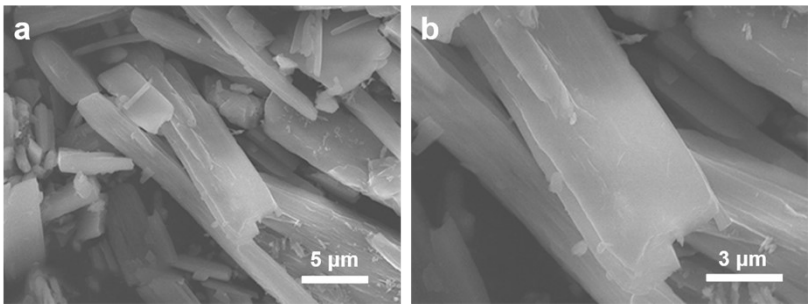

Fig. S2. SEM images of Zn-BTC at different magnifications showing a rod-like morphology.

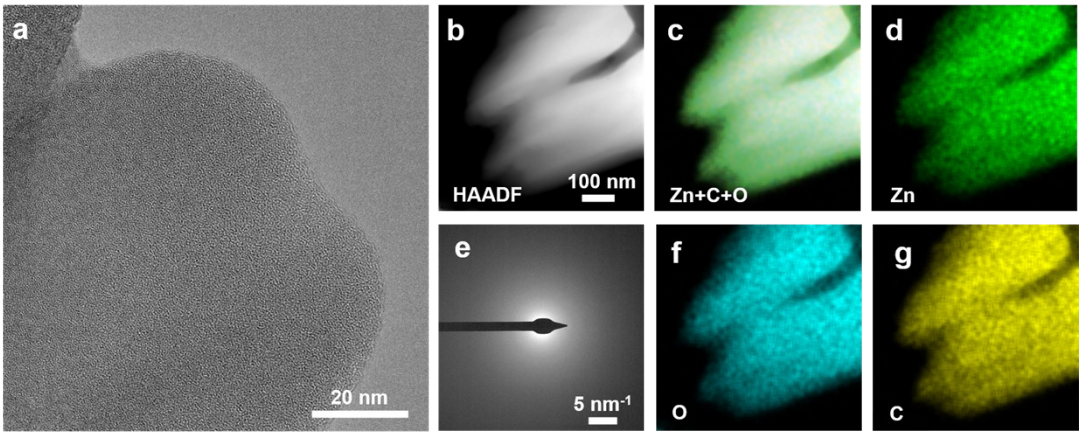

Fig. S3. (a) BF-STEM image of Zn-BDC. (b-d, f, g) HAADF-STEM image and corresponding EDS elemental maps of Zn-BDC, suggesting a uniform distribution of Zn, O, C. (e) SAED pattern of Zn-BDC.

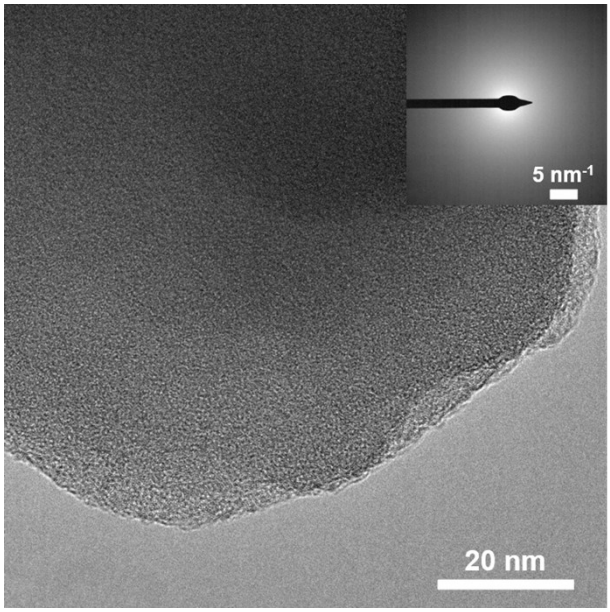

Fig. S4. BF-STEM image and SAED pattern (insert) of Zn-BTC, in which Zn-BTC appears to be amorphous as a result of the sensitivity of MOFs to the electron beam.

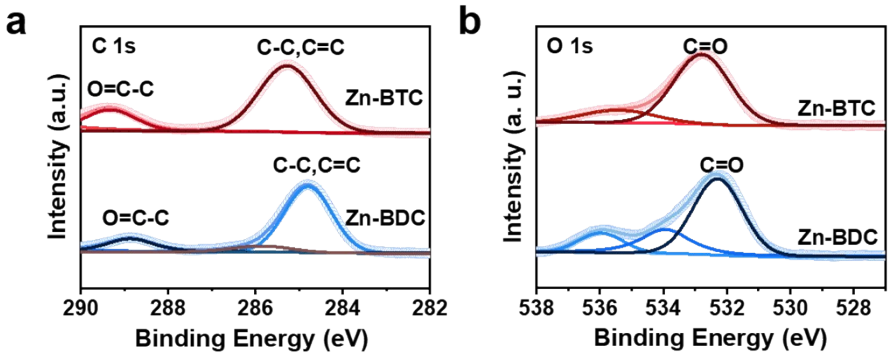

Fig. S5. (a) C 1s and (b) O 1s XPS spectra of Zn-BTC and Zn-BDC, suggesting the existence of carboxyl groups.

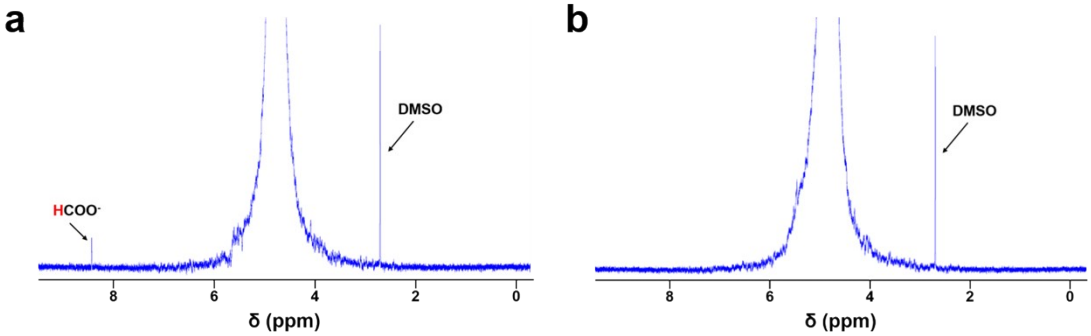

Fig. S6. Typical quantitative ^{1}H NMR spectra of liquid product for Zn-BTC in 1 M $KHCO_3$ (a) and 1 M KOH (b).

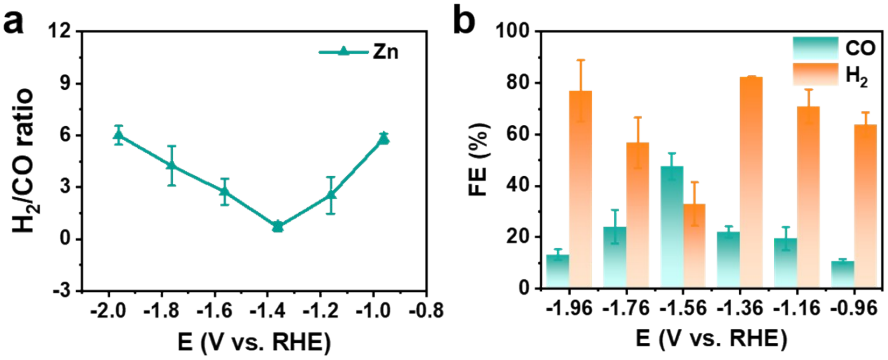

Fig. S7. (a) The molar ratio between H_2 and CO vs. the applied potential for Zn powder. (b) Potential-dependent CO and H_2 FEs of Zn powder.

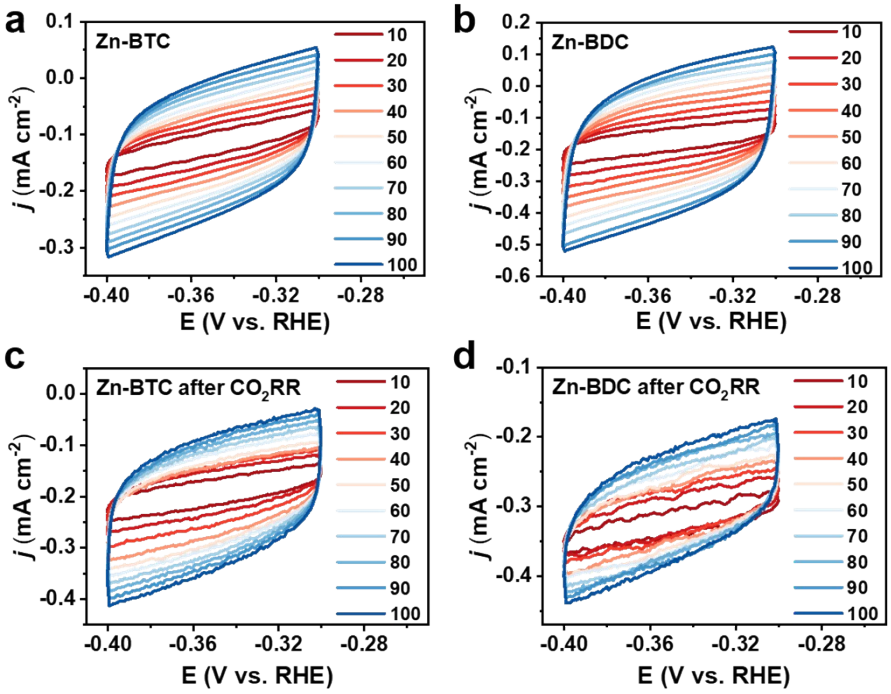

Fig. S8. Capacitive behaviors on the prepared Zn-MOFs electrodes. Measured cyclic voltammetry (CV) on the (a) Zn-BTC, (b) Zn-BDC, (c) Zn-BTC after CO_2RR, and (d) Zn-BDC after CO_2RR electrodes with a potential range from –0.3 to –0.4 V in a CO_2-bubbled 1 M $KHCO_3$ electrolytes. Notes: The unit of 10-100 is mV s^{-1}.

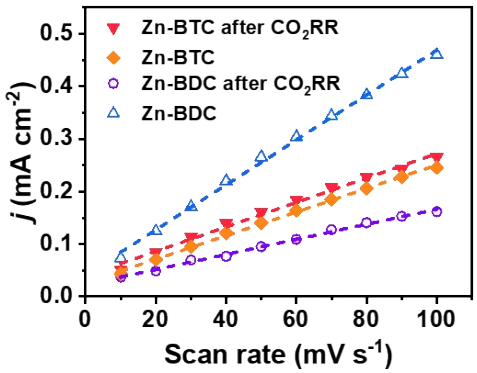

Fig. S9. The linear regression of the double-layer capacitance of Zn-BTC and Zn-BDC before and after CO_2RR obtained from the electrochemical studies. Double-layer capacitance (C_{dl}) of catalysts were obtained by measuring CV in the potential ranges

between −0.3 and −0.4 V vs. RHE where no Faradaic process occurred at scan rates from 10 to 100 mV s^{-1}. The CV measurement was operated in the flow-cell reactor and 1 M $KHCO_3$ was used as the electrolytes. During the measurement, CO_2 was continuously supplied to the electrolytes. By plotting the average current Δj ($\Delta j=(j_{anodic}-j_{cathodic})/2$ at −0.35 V vs. RHE) against the scan rate, C_{dl} value was given by the slope and the corresponding results are displayed in Table S1.[3]

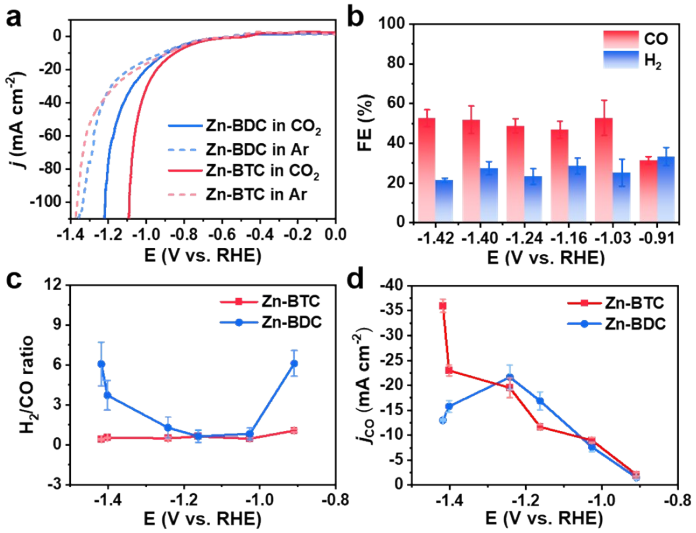

Fig. S10. *iR*-corrected CO_2RR performance in 1 M $KHCO_3$. (a) LSV curves of Zn-BTC and Zn-BDC in CO_2 and Ar atmosphere. (b) Potential-dependent CO and H_2 FEs of Zn-BTC. (c) The molar ratio between H_2 and CO vs. the applied potential. (d) j_{CO} vs. the applied potential.

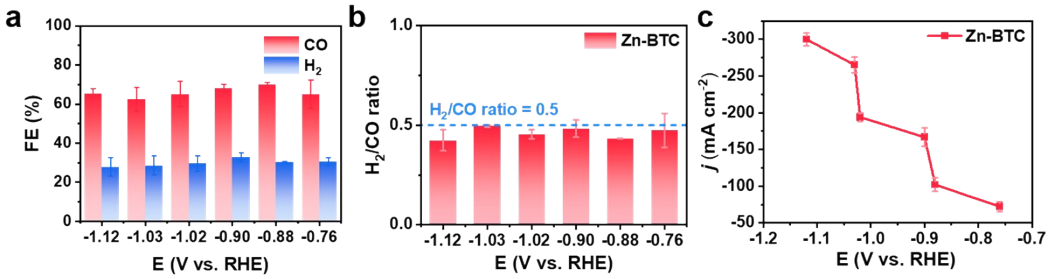

Fig. S11. *iR*-corrected CO_2RR performance in 1 M KOH. (a) Potential-dependent CO and H_2 FEs of Zn-BTC. (b) The molar ratio between H_2 and CO vs. the applied potential. (c) Current density vs. the applied potential.

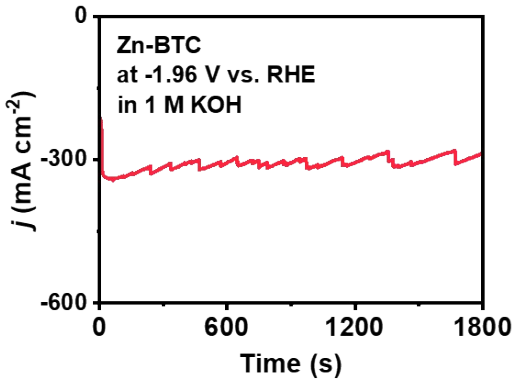

Fig. S12. *j* vs. reaction time for Zn-BTC at −1.96 V vs. RHE in 1 M KOH.

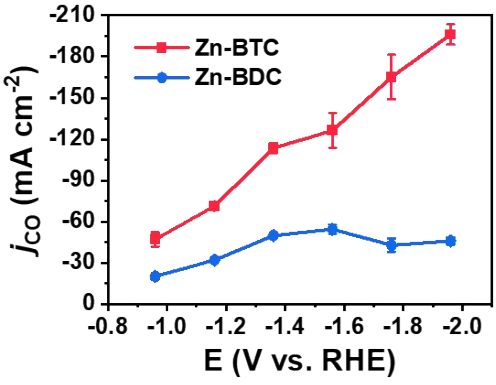

Fig. S13. j_{CO} vs. the applied potential for Zn-BTC and Zn-BDC in 1 M KOH, showing that Zn-BTC exhibits superior CO_2 electroreduction performance over Zn-BDC.

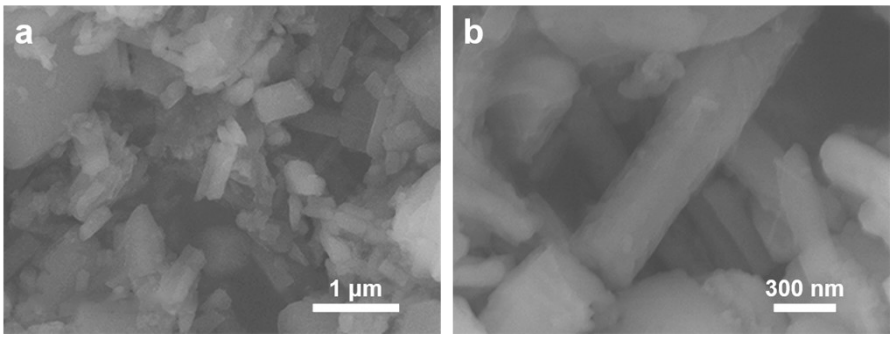

Fig. S14. SEM images of Zn-BTC after electrolysis at different magnifications showing the maintenance of the rod-like morphology.

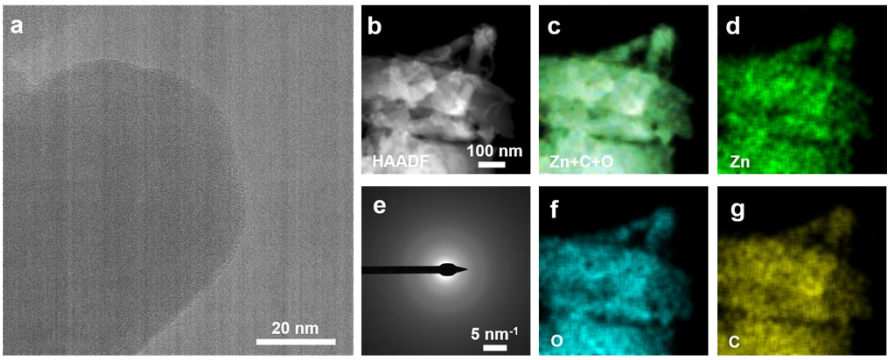

Fig. S15. (a) BF-STEM image of Zn-BTC after electrolysis showing an amorphous structure similar to the as-prepared catalyst. (b-d, f, g) HAADF-STEM image and corresponding elemental maps of Zn-BTC after electrolysis, suggesting a uniform distribution of Zn, O, C. (e) SAED pattern of Zn-BTC after electrolysis.

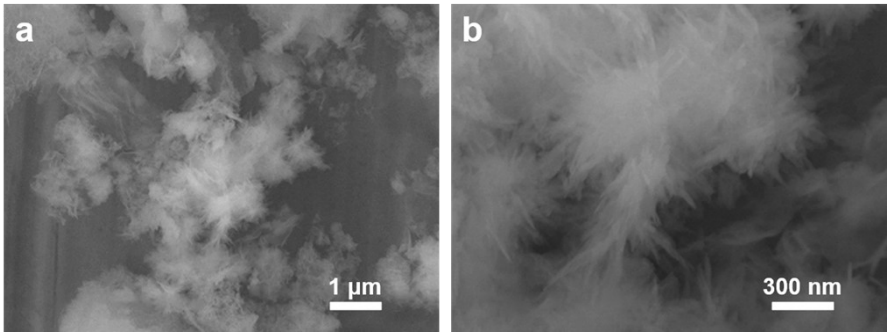

Fig. S16. SEM images of Zn-BDC after electrolysis at different magnifications showing the rod-like morphology changed to a flocculent one.

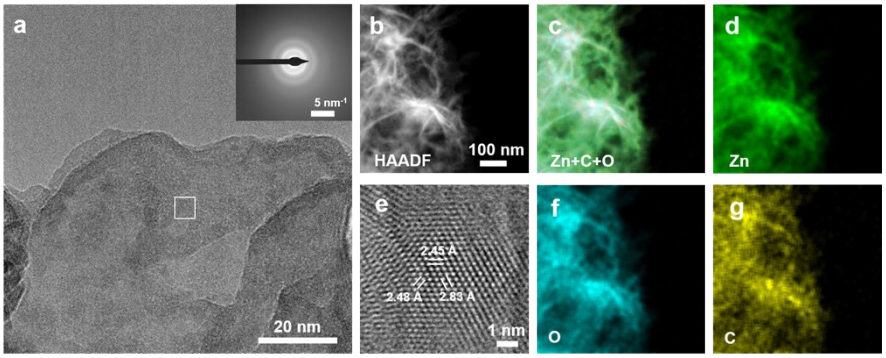

Fig. S17. (a) BF-STEM image and SAED pattern (insert) of Zn-BDC after electrolysis showing a clear crystalline structure. (b-d, f, g) HAADF-STEM image and corresponding EDS elemental maps of Zn-BDC after electrolysis. (e) Magnified BF-STEM image of Zn-BDC after electrolysis, suggesting partial reduced Zn-BDC.

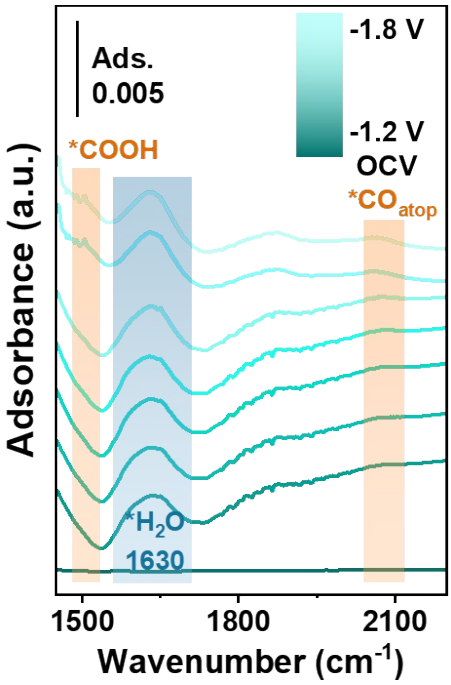

Fig. S18. ATR-SEIRAS spectra of Zn, indicating that it is easier for $^{*}H_2O$ to be adsorbed on Zn than CO_2 intermediates.

Table S1. The relationship between FE(formate) and applied potentials for Zn-BTC in different electrolytes obtained from quantitative ^{1}H NMR spectra.

E (V vs. RHE)	FE(formate) in $KHCO_3$	FE(formate) in KOH
−0.96	11.5	0
−1.16	21.0	0
−1.36	20.7	0
−1.56	22.5	0
−1.76	16.8	0
−1.96	17.8	0

Table S2. Double-layer capacitance (C_{dl}) of catalysts under different conditions.

Sample	Atmosphere	C_{dl} (mF cm^{-2})	R^2
Zn-BTC	CO_2	1.12	0.99
Zn-BTC after CO_2RR	CO_2	1.16	0.99
Zn-BDC	CO_2	2.13	0.99
Zn-BDC after CO_2RR	CO_2	0.72	0.99

Notes: The C_{dl} were obtained by measuring CV in the potential ranges between −0.3 and −0.4 V vs. RHE where no Faradaic process occurred at scan rates from 10 to 100 mV s^{-1}.

Table S3. Turnover frequencies (TOF) of Zn-MOFs under different conditions.

E (V vs. RHE)	TOF (s^{-1})			
	Zn-BTC		Zn-BDC	
	1 M $KHCO_3$	1 M KOH	1 M $KHCO_3$	1 M KOH
−0.96	0.0013	0.0290	0.0008	0.0106
−1.16	0.0055	0.0439	0.0040	0.0169
−1.36	0.0072	0.0698	0.0089	0.0264
−1.56	0.0120	0.0777	0.0115	0.0288
−1.76	0.0141	0.1016	0.0084	0.0227
−1.96	0.0221	0.1207	0.0069	0.0243

Notes: The initial number of Zn sites was used throughout in calculations.

References

1. J. Heyes, M. Dunwell and B. Xu, *J. Phys. Chem. C*, 2016, **120**, 17334-17341.
2. C. Yan, H. Li, Y. Ye, H. Wu, F. Cai, R. Si, J. Xiao, S. Miao, S. Xie, F. Yang, Y. Li, G. Wang and X. Bao, *Energy Environ. Sci.*, 2018, **11**, 1204-1210.
3. W. Luo, J. Zhang, M. Li and A. Züttel, *ACS Catal.*, 2019, **9**, 3783-3791.